

The natural synovial joint: properties of cartilage

G A Ateshian^{1*} and C T Hung²

¹Departments of Mechanical Engineering and Biomedical Engineering, Columbia University, New York, USA

²Department of Biomedical Engineering, Columbia University, New York, USA

The manuscript was received on 31 May 2005 and was accepted after revision for publication on 5 May 2006.

DOI: 10.1243/13506501JET86

Abstract: Articular cartilage is the bearing material that lines the ends of the bones of synovial joints. Its primary function is to reduce friction and wear at the articulations of the musculoskeletal system. The tribological properties of cartilage are intimately related to its structure and mechanical properties. The modes of lubrication in cartilage extend beyond the traditional mechanisms of fluid-film or boundary lubrication. The purpose of this review is to describe the salient properties of articular cartilage necessary to understand the unique biotribology of diarthrodial joints.

Keywords: cartilage, mixture theory, interstitial fluid pressurization, biotribology

1 CARTILAGE STRUCTURE AND FUNCTION

Cartilage is a white connective tissue which is synthesized and maintained by cells called chondrocytes (Fig. 1). In human joints, the thickness of the articular cartilage layer varies from 0.5 to 1.5 mm in upper extremity joints, such as the hand and the shoulder [1, 2], and from 1 to 6 mm in lower extremity joints, such as the hip, knee, and ankle [3–5]. Under normal conditions, articular cartilage provides low friction and wear over a life span. It is a highly hydrated tissue, with a porosity varying from 68 to 85 per cent in adult joints [6, 7]. The interstitial fluid of cartilage is water, containing electrolytes such as sodium and chloride.

Cartilage cells only occupy about 5 per cent of the tissue volume. The surrounding tissue matrix (the extracellular matrix of cartilage) consists primarily of a protein called collagen type II (10–20 per cent of the wet weight) and proteoglycans (5–10 per cent of the wet weight) [6, 7]. The collagen has a fibrillar structure which is well suited to sustain tensile stresses. These fibrils, whose diameter varies from 10 to 300 nm, exhibit a different orientation through the depth of the tissue from the articular

surface to the subchondral bone (the bone right below the cartilage, onto which it is anchored). In the superficial tangential zone, which consists of 10–20 per cent of the topmost region of the articular layer, the fibrils are oriented parallel to the articular surface. In the middle zone, which consists of the next 40–60 per cent of the thickness, their orientation is more random, whereas, in the deep zone their orientation is perpendicular to the bony surface. This heterogeneity in the ultrastructural organization of the collagen matrix is reflected in the heterogeneity of tensile properties through the depth, as discussed subsequently. When the cartilage surface is pricked with a needle, the tissue splits along a direction known as the split-line direction, which represents the predominant collagen fibril orientation.

Proteoglycans are macromolecules consisting of proteins and sugars, which aggregate together by linking non-covalently to a hyaluronan backbone, forming very large macromolecules called aggrecans. Proteoglycans consist primarily of negatively charged glycosaminoglycan (GAG) chains (sugars) covalently linked to a protein core. Proteoglycans are typically enmeshed and immobilized within the collagen matrix. Consequently, the negative charges on their GAG chains are referred to as the tissue's fixed-charge density (FCD). As these negative charges cannot freely flow out of the tissue, the interstitial fluid must contain an excess of cations, relative to the external bathing solution, in order to maintain

*Corresponding author: Departments of Mechanical Engineering and Biomedical Engineering, Columbia University, 500 West 120th Street, MC4703, 220 S. W. Mudd, New York, NY 10027, USA. email: ateshian@columbia.edu

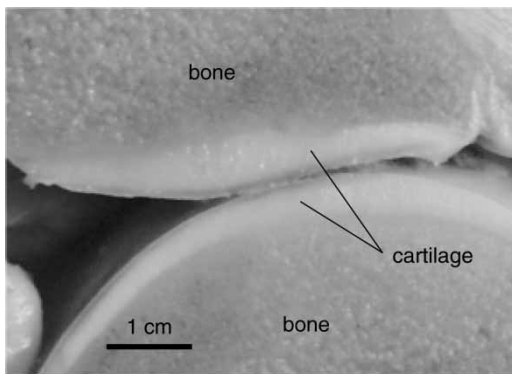


Fig. 1 Cross-section of the patellofemoral joint from a human knee, showing the articular layers and subchondral bone of the patella (top) and femoral trochlea

electroneutrality within the tissue. The net effect is that the osmolarity of ions inside the tissue is greater than outside, producing an osmotic pressure within the interstitial fluid [8–10]. This Donnan osmotic pressure increases with increasing FCD, and the FCD increases with compressive strain, as the charges get closer together. The rate of change of osmotic pressure with compressive strain may be construed as an osmotic modulus; hence, the proteoglycans of cartilage contribute to the tissue's compressive properties [9, 11].

While the cartilage porosity is quite elevated, the tightly entangled collagen fibrils and proteoglycan molecules contribute to produce a very small effective pore size for the cartilage matrix, estimated to be on the order of 1 nm. Therefore, the permeability of cartilage, which measures the resistance to interstitial fluid flow in the presence of a pressure gradient, is very small. Compared with artificial 'self-lubricating' or 'oil-retaining' porous bearings, the high porosity, low permeability, and relatively low modulus of cartilage makes it a unique bearing material.

2 GOVERNING EQUATIONS FOR CARTILAGE

From basic principles of continuum mechanics, it is well known that the mechanical properties of a material can only be identified and measured once a suitable constitutive model has been formulated. The formulation of a constitutive model is an iterative theoretical process based on experimental observations. It has been known from permeation experiments that water flows through cartilage [12–15], and that the energy dissipated by this interstitial fluid flow results in a flow-dependent viscoelasticity [16]. These classical studies have since been supported by overwhelming experimental data which

indicate that articular cartilage needs to be modelled using porous media theories to account for the pressurization and flow of the interstitial fluid within the solid collagen–proteoglycan matrix during tissue loading. One of the earliest and most widely used successful porous media models of articular cartilage is the biphasic theory of Mow *et al.* [17], which uses the framework of mixture theory [18–20] to describe cartilage as a mixture of an intrinsically incompressible solid and an intrinsically incompressible fluid. This mixture approach has also been successfully extended to incorporate the FCD in the solid matrix and electrolytes in the interstitial fluid [9, 21, 22]. In the mixture approach, the total stress in the tissue, σ , represents the superposition of the hydrostatic interstitial fluid pressure, p , and extra stress in the solid matrix, σ^e

$$\sigma = -pI + \sigma^e \quad (1)$$

where I is the identity tensor. The extra stress is a function of the tissue strain. In this review, only infinitesimal strain theory is discussed, with the infinitesimal strain tensor given by $E = (\text{grad } \mathbf{u} + \text{grad}^T \mathbf{u})/2$, where \mathbf{u} is the solid matrix displacement. Under quasi-static conditions, which prevail for most loading configurations of cartilage, and in the absence of external body forces, the conservation of linear momentum requires that

$$\text{div } \sigma = 0 \quad (2)$$

2.1 Solid matrix stresses

Many different forms have been proposed for the constitutive relation between σ^e and E , depending on the specific experimental phenomena that needed to be captured. When testing cartilage in confined compression [17, 23] or indentation [24–26], the classical linear isotropic elastic relation has often been found suitable

$$\sigma^e = \lambda(\text{tr}E)I + 2\mu E \quad (3)$$

where λ and μ are the Lamé constants of the solid matrix. The confined compression modulus is called the aggregate modulus [17] and is given by $H_A = \lambda + 2\mu$, whereas μ is the shear modulus.

The constitutive relation of equation (3) predicts that the tissue properties are isotropic and identical in tension and compression. However, experiments have shown that articular cartilage exhibits markedly higher moduli in tension versus compression [27–30], which has motivated several investigators to adopt a more general constitutive relation to capture this behaviour [31–34]. Furthermore, the tensile

modulus measured parallel to the split-line direction has been reported to be approximately twice as high as that measured perpendicular to the split-line direction [27, 35], suggesting that cartilage exhibits orthotropic symmetry [29, 36]. Using the frame-invariant conewise linear elasticity (CLE) theory of Curnier *et al.* [37], the tension–compression non-linearity and orthotropic symmetry can be modelled with

$$\boldsymbol{\sigma}^e = \sum_{a=1}^3 \left[\lambda_{aa} \{ \text{tr} \mathbf{A}_a \mathbf{E} \} (\text{tr} \mathbf{A}_a \mathbf{E}) \mathbf{A}_a + \boldsymbol{\mu}_a (\mathbf{A}_a \mathbf{E} + \mathbf{E} \mathbf{A}_a) + \sum_{\substack{b=1 \\ b \neq a}}^3 \lambda_{ab} \text{tr} (\mathbf{A}_a \mathbf{E}) \mathbf{A}_b \right] \quad (4)$$

The texture tensors appearing in this relation, $\mathbf{A}_a = \mathbf{a}_a \otimes \mathbf{a}_a$, are dyadic products of the unit vectors \mathbf{a}_a oriented parallel ($a = 1$) and perpendicular ($a = 2$) to the split-line direction, and normal to the articular surface ($a = 3$). The tension–compression non-linearity is captured by the functional dependence of λ_{aa} on $\text{tr} \mathbf{A}_a \mathbf{E}$, which is the normal strain component along the vectors \mathbf{a}_a

$$\lambda_{aa} \{ \text{tr} \mathbf{A}_a \mathbf{E} \} = \begin{cases} \lambda_{-aa} & \text{tr} \mathbf{A}_a \mathbf{E} < 0 \\ \lambda_{+aa} & \text{tr} \mathbf{A}_a \mathbf{E} > 0 \end{cases} \quad (5)$$

λ_{-aa} and λ_{+aa} represent the moduli when the normal strain is compressive and tensile, respectively. Note that $\lambda_{ba} = \lambda_{ab}$, so that the total number of material constants for this tension–compression orthotropic model is 12 (three more than in the classical case of linear orthotropic elasticity). Tensile and compressive aggregate moduli can also be defined $H_{\pm Aa} = \lambda_{\pm aa} + 2\boldsymbol{\mu}_a$; for example, $H_{+A1} = \lambda_{+11} + 2\boldsymbol{\mu}_1$ is the tensile aggregate modulus along the split-line direction and H_{-A3} is the compressive aggregate modulus along the thickness direction.

In problems where it is less important to capture the orthotropic symmetry than the tension–compression non-linearity, the symmetry can be raised to become cubic, by letting $\lambda_{+aa} \equiv \lambda_{+1}$, $\lambda_{-aa} \equiv \lambda_{-1}$ (or equivalently, $H_{\pm Aa} \equiv H_{\pm A}$), $\lambda_{ab} \equiv \lambda_2$, and $\boldsymbol{\mu}_a \equiv \boldsymbol{\mu}$ ($a, b = 1-3$) [34]. This cubic symmetry model has four material constants, H_{+A} , H_{-A} , λ_2 , and $\boldsymbol{\mu}$. These material constants may be related to the tensile and compressive Young’s moduli, $E_{\pm Y}$, and Poisson’s ratios, ν_{\pm} , through a generalized form of the classical linear isotropic elasticity relations

$$E_{\pm Y} = H_{\pm A} - \frac{2\lambda_2^2}{H_{\pm A} + \lambda_2}, \quad \nu_{\pm} = \frac{\lambda_2}{H_{\pm A} + \lambda_2} \quad (6)$$

The constitutive models of equations (3) and (4) assume that the solid matrix behaves elastically, so that the viscoelastic response of the solid–fluid mixture derives entirely from the energy dissipation due to interstitial fluid flow, also called flow-dependent viscoelasticity. These types of constitutive models can explain the observed time-dependent response of cartilage loaded in confined and unconfined compression, and indentation. However, these models predict a time-invariant elastic response to torsional loading of a cylindrical disc [34] and a nearly time-invariant elastic response in uniaxial tension [38]. Neither of these predictions is supported by experimental measurements, which show significant time-varying viscoelastic responses in these loading configurations [39–43]. Consequently, several investigators have proposed that the solid matrix is also intrinsically viscoelastic [38, 39, 44–46], which implies that energy dissipation occurs in the collagen–proteoglycan matrix as a result of the breaking and reforming of (presumably non-covalent) molecular bonds. This flow-independent viscoelasticity has been commonly modelled using the quasi-linear viscoelastic model of Fung [47]

$$\boldsymbol{\sigma}^{ve}(t) = g(t) \boldsymbol{\sigma}^e \{ \mathbf{E}(0) \} + \int_0^t g(t - \tau) \frac{\partial \boldsymbol{\sigma}^e}{\partial \tau} \{ \mathbf{E}(\tau) \} d\tau \quad (7)$$

where $\boldsymbol{\sigma}^{ve}$ is the viscoelastic stress in the solid matrix and $\boldsymbol{\sigma}^e$ the equilibrium elastic response given for example by equation (3) or (4). In this case, the total mixture stress is given by $\boldsymbol{\sigma} = -p\mathbf{I} + \boldsymbol{\sigma}^{ve}$, which supersedes equation (1). $g(t)$ is a suitably chosen relaxation function, such as

$$g(t) = 1 + c \left[E_i \left(\frac{t}{\tau_2} \right) - E_i \left(\frac{t}{\tau_1} \right) \right] \quad (8)$$

where $E_i(\cdot)$ is the exponential integral function and c , τ_1 , and τ_2 are material coefficients [47]. The value of the relaxation function upon instantaneous loading is of particular significance and is given by $g(0^+) = 1 + c \ln(\tau_2/\tau_1)$, whereas the long-term response is given by $g(\infty) = 1$.

It follows from this presentation that articular cartilage exhibits both flow-dependent and flow-independent viscoelasticity. Therefore, under dynamic loading conditions, the dynamic tensile, compressive, and shear moduli are significantly greater than their corresponding equilibrium moduli appearing in the constitutive relations given earlier. The dynamic moduli vary with the loading frequency f ; furthermore, with regard to flow-dependent viscoelasticity, the frequency response is a function of the dimensions of the tissue sample because flow-dependent effects are regulated by the path length

required for interstitial fluid to exude from the tissue. For example, in unconfined compression of a cylindrical tissue sample between impermeable loading platens, the characteristic loading frequency for flow-dependent viscoelasticity is given by $f_c = H_{\pm A} k / a^2$, where a is the sample radius and k the hydraulic permeability described in the next section. At this characteristic frequency, the energy dissipation resulting from the diffusive drag between the interstitial fluid and the solid matrix is greatest. When $f \ll f_c$, interstitial fluid pressurization is negligible, the fluid flows through the solid matrix with negligible resistance, and the tissue behaves as a compressible solid; when $f \gg f_c$, the interstitial fluid pressure reaches its maximum value, the fluid has little time to flow relative to the solid matrix, and the tissue behaves as an incompressible solid. The intrinsic viscoelastic behaviour is superposed upon this flow-dependent response. When $1/\tau_2 \leq f \leq 1/\tau_1$, the energy dissipation from intrinsic solid matrix viscoelasticity is greatest; at the two extremes, $f \ll 1/\tau_2$ and $f \gg 1/\tau_1$, the tissue behaves elastically. On the basis of the constitutive relations for cubic symmetry, the upper bounds on the dynamic tensile and compressive Young's moduli and Poisson's ratios, which occur when $f \gg f_c$ and $f \gg 1/\tau_1$, are given by reference [38]

$$E_{\pm Y}^{0+} = \left(1 + c \ln \frac{\tau_2}{\tau_1}\right) \left(H_{\pm A} - \frac{3}{2} \lambda_2 + \frac{H_{\pm A}}{2}\right);$$

$$v_{\pm}^{0+} = \frac{1}{2} \quad (9)$$

The term in the first parenthesis represents the dynamic enhancement factor resulting from flow-independent viscoelasticity, whereas the term in the second parenthesis represents the dynamic modulus resulting from flow-dependent effects. The value of the dynamic Poisson's ratio confirms that the tissue behaves as an incompressible solid at sufficiently high frequencies. At the other end of the frequency spectrum, when $f \ll f_c$ and $f \ll 1/\tau_2$, the corresponding moduli are given in equation (6).

Before concluding this section on constitutive models for solid matrix stresses, it is of interest to note that these constitutive relations for infinitesimal strains remain essentially unchanged when modelling the FCD of the solid matrix and incorporating electrolytes in the interstitial fluid [9, 11, 48]. When the interstitial fluid contains two monovalent counter-ions, the osmotic modulus Π resulting from the rate of change of Donnan osmotic pressure with dilation is given (under ideal conditions) by

$$\Pi = \frac{R\theta(c_r^F)^2}{\phi_r^w \sqrt{(c_r^F)^2 + (2c^*)^2}} \quad (10)$$

where c_r^F is the FCD and ϕ_r^w is the tissue porosity, in the reference state of zero strain, R the universal gas constant, θ the absolute temperature, and c^* the salt concentration in the external bath [11]. Within the CLE framework of equation (4), the osmotic modulus is superposed upon the material coefficients $\lambda_{\pm aa}$ (or $H_{\pm Aa}$) and λ_{ab} ; this means that the explicit incorporation of the osmotic modulus into equation (4) is simply achieved by substituting $\lambda_{\pm aa}^{\text{eff}} = \lambda_{\pm aa} + \Pi$ for $\lambda_{\pm aa}$ (or $H_{\pm Aa}^{\text{eff}} = H_{\pm Aa} + \Pi$ for $H_{\pm Aa}$) and $\lambda_{ab}^{\text{eff}} = \lambda_{ab} + \Pi$ for λ_{ab} . These 'effective' properties represent the combination of the osmotic modulus with the structural moduli of the collagen-proteoglycan matrix, which are independent of the osmotic modulus. This formulation provides an explicit dependence of the material properties of the solid matrix on the FCD and external bath concentration. The relation of equation (10) shows that Π increases with increasing c_r^F and decreases with increasing c^* .

2.2 Solid matrix permeability

In addition to the conservation of linear momentum for the mixture (equation (2)), it is necessary to satisfy the conservation of linear momentum for the interstitial fluid. In the absence of fixed charges, and under the assumption that the frictional drag between the interstitial fluid and the solid matrix is linearly proportional to their relative velocity, the momentum equation for the interstitial fluid reduces to Darcy's law

$$\mathbf{w} = -k \text{grad } p \quad (11)$$

where \mathbf{w} is the volumetric flux of water relative to the solid matrix, and k the hydraulic permeability. This formulation assumes that the permeability is isotropic; a more general formulation may be given by $\mathbf{w} = -\mathbf{k} \text{grad } p$, where \mathbf{k} is the permeability tensor whose spectral representation is $\mathbf{k} = \sum_{a=1}^3 k_a \mathbf{A}_a$. Thus, k_1 , k_2 , and k_3 represent the permeability parallel and perpendicular to the split-line direction, and normal to the articular surface, respectively. To complete the set of governing equations for a solid-fluid mixture, the conservation of mass for the mixture needs to be satisfied

$$\text{div}(\mathbf{v}^s + \mathbf{w}) = 0 \quad (12)$$

where \mathbf{v}^s is the velocity of the solid matrix, related to the displacement through the material derivative with respect to the solid, $\mathbf{v}^s = D^s \mathbf{u} / Dt$.

In the presence of fixed charges, the flux of water and ions is more complex and the full treatment is beyond the scope of this presentation. However,

under zero current (one-dimensional open circuit conditions), the effective permeability is given by

$$k^{\text{eff}} = k \left(1 + \frac{2kR\theta(c_r^F)^2}{\varphi_r^v \left[(D^+ - D^-)c_r^F + (D^+ + D^-) \times \sqrt{(c_r^F)^2 + (2c^*)^2} \right]} \right)^{-1} \quad (13)$$

where k represents the intrinsic hydraulic permeability of the matrix independent of the effect of fixed charges [49]; D^+ and D^- are the diffusivities of the monovalent counter-ions (sodium and chloride) in the interstitial fluid. In this case, $\mathbf{w} = -k^{\text{eff}} \text{grad } p$ supersedes equation (11). This result shows that the effective permeability of the tissue decreases with increasing FCD.

3 CARTILAGE MATERIAL PROPERTIES

Experimental measurements of the mechanical properties of cartilage are performed either *in situ*, whereby the articular layer is left intact on its subchondral bone, or on explants isolated from the articular layer. All measurements need to be performed in a saline solution, typically supplemented with protease inhibitors to retard tissue degradation over long testing durations; the solution may be buffered to maintain a physiological pH; the NaCl concentration is typically physiological, 0.15 M, but it may be varied to investigate the corresponding variations in the material properties.

In situ measurements typically consist of indenting the articular cartilage with a flat-ended or hemispherical probe which is either impermeable, or porous and free draining (Fig. 2) [26, 50–52]. *In situ* measurements offer the advantage of keeping the tissue intact, though the contact indentation analysis required to recover the intrinsic material properties is more complex [24, 25, 53, 54]. Most indentation analyses have been performed using the constitutive relation of equation (3) for the solid matrix stresses, and equation (11) for the permeability; the material properties recovered from these analyses are H_A , ν (or μ), and k , where H_A is typically representative of the compressive aggregate modulus along the direction normal to the articular surface, H_{-A3} . Indentation results have been reported for human cartilage and for many animal

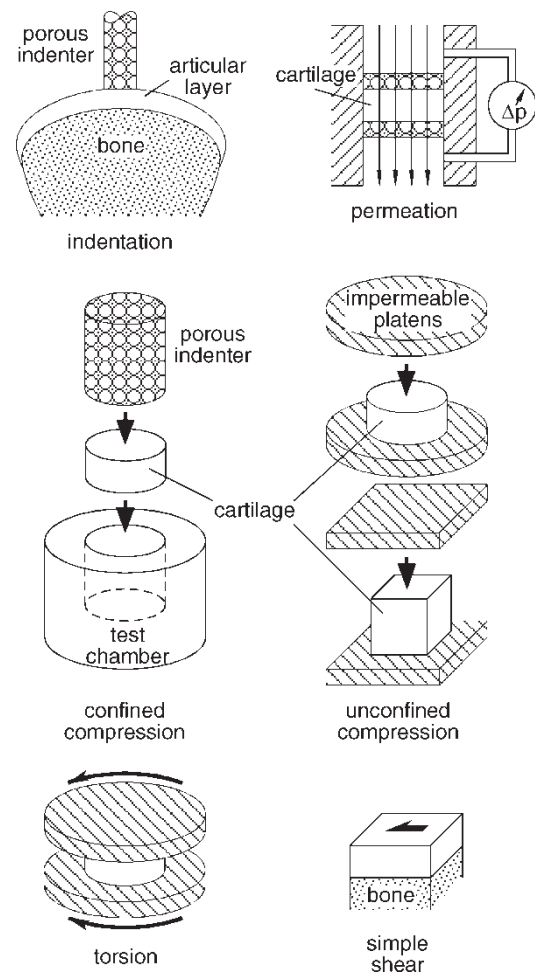


Fig. 2 Common testing configurations for articular cartilage. All experiments are generally conducted with the tissue immersed in saline

species [26, 55–60]. Typical values for normal human cartilage are $H_A \sim 0.5\text{--}0.7$ MPa, $\nu \sim 0.0\text{--}0.1$, and $k \sim (1.1\text{--}2.2) \times 10^{-15}$ m⁴/N s [26].

Experimental measurements on tissue explants typically consist of permeation tests [12–15], confined compression [17, 28, 61, 62], unconfined compression [15, 63–67], simple shear [39], and torsional shear [34, 41, 68]. The advantages of testing explants include the ability to extract material properties from a simpler analysis, the ability to measure inhomogeneous properties through the thickness of the articular layer, and the ability to measure properties along the principal texture directions of the tissue.

Permeation tests consist of applying a pressure gradient across a cylindrical cartilage sample and measuring the resulting fluid flux, or driving the fluid at a prescribed velocity (using a syringe pump [69]) and measuring the pressure drop between upstream and downstream (Fig. 2). The permeability measured from permeation tests has been found

to decrease from the articular surface, where $k \sim (0.3\text{--}0.7) \times 10^{-15} \text{ m}^4/\text{N s}$, to the deep zone, where $k \sim (0.15\text{--}0.25) \times 10^{-15} \text{ m}^4/\text{N s}$ [8]. The permeability measured tangentially to the articular surface (k_1 or k_2) is similar to that measured normal to the articular surface (k_3) [70], supporting the premise of an isotropic permeability tensor. The permeability significantly decreases with increasing tissue compression [14], as may be described by an exponential function, $k = k_0 \exp(M \text{ tr } E)$ [23, 71], where k_0 is the permeability in the limit of zero dilatation and M is the non-linear permeability coefficient. Typical values are $k_0 \sim 1.7 \times 10^{-15} \text{ m}^4/\text{N s}$ and $M \sim 4.3$ [71].

In confined compression, a cylindrical tissue sample is placed in a chamber of the same diameter, with an impermeable side wall; the tissue is loaded with a free-draining porous indenter of nearly the same diameter to allow uniaxial tissue deformation and fluid exudation upon tissue compression (Fig. 2). The compressive aggregate modulus can be determined from the equilibrium stress–strain response, whereas the permeability can be obtained by curve-fitting the transient response. For example, for human patellar cartilage, $H_A = 0.79 \pm 0.36 \text{ MPa}$ and $k = (4.7 \pm 3.6) \times 10^{-15} \text{ m}^4/\text{N s}$ for full-thickness samples [28]. When incorporating intrinsic viscoelasticity of the solid matrix, as per equations (7) and (8), reported values for bovine cartilage are $H_A = 0.54 \pm 0.25 \text{ MPa}$, $k = (50 \pm 35) \times 10^{-15} \text{ m}^4/\text{N s}$, $c = 0.39 \pm 0.22$, $\tau_1 = 0.06 \pm 0.08 \text{ s}$, and $\tau_2 = 8.0 \pm 7.1 \text{ s}$ [45]. The values observed for the hydraulic permeability from curve-fitting the transient response of confined compression tests are often higher than direct measurements from permeation tests, particularly when incorporating solid matrix intrinsic viscoelasticity. This outcome suggests that indirect measures of permeability are sensitive to the curve-fitting procedure and the constitutive assumptions for the solid matrix stresses. Using optical techniques, it is also possible to measure the local strain distribution through the thickness of the articular layer, to yield depth-dependent values of H_A [72]. Such measurements have demonstrated that the compressive aggregate modulus of cartilage is smallest at the articular surface and increases monotonically toward the deep zone, from 0.04 to 2.1 MPa in the case of mature bovine articular cartilage [72].

Unconfined compression measurements consist of loading a cartilage sample between two impermeable platens (Fig. 2). The equilibrium stress–strain response yields the compressive Young's modulus along the loading direction. Optical measurements of the equilibrium lateral and axial strains can be used to measure Poisson's ratio [73–75]. An added advantage of unconfined compression is that tissue samples can be cut into small cubes, so that Young's moduli and Poisson's ratios can be

measured along three mutually perpendicular directions [36]. For example, in bovine cartilage, it has been reported that $E_{-Y1} = 0.38 \pm 0.10 \text{ MPa}$, $E_{-Y2} = 0.38 \pm 0.13 \text{ MPa}$, and $E_{-Y3} = 0.87 \pm 0.37 \text{ MPa}$ [36]. Depth-dependent measurements of Young's modulus and Poisson's ratio in compression demonstrate that both are smallest at the articular surface and increase towards the deep zone; for example, in immature bovine cartilage, ν_- increases from 0.05 to 0.2 [75].

Curve-fitting of the transient unconfined compression response may be used to estimate the permeability and tensile modulus tangential to the loading direction as well as Poisson's ratio [32, 34, 76]. However, as the number of material constants governing the response of a particular experiment increases, it becomes necessary to perform multiple tests on the same tissue sample to provide more reliable estimates of these properties. For example, in a study of immature bovine cartilage, confined and unconfined compression tests of the same tissue sample were combined to yield values of five material coefficients: $H_{-A3} = 0.64 \pm 0.22 \text{ MPa}$, $H_{+A1} \approx H_{+A2} = 13.2 \pm 1.7 \text{ MPa}$, $\lambda_2 = 0.48 \pm 0.23 \text{ MPa}$, $k_3 = (0.36 \pm 0.10) \times 10^{-15} \text{ m}^4/\text{N s}$, and $k_1 \approx k_2 = (0.61 \pm 0.21) \times 10^{-15} \text{ m}^4/\text{N s}$ [34]. To explore the role of intrinsic solid matrix viscoelasticity, another study performed one confined compression and two unconfined compression tests (using slow and fast loading rates) on the same tissue sample, to yield eight material coefficients for immature bovine cartilage: $H_{-A3} = 0.51 \pm 0.18 \text{ MPa}$, $H_{+A1} \approx H_{+A2} = 8.8 \pm 2.5 \text{ MPa}$, $\lambda_2 = 0.30 \pm 0.13 \text{ MPa}$, $k_3 = (1.44 \pm 0.89) \times 10^{-15} \text{ m}^4/\text{N s}$, $k_1 \approx k_2 = (1.07 \pm 0.46) \times 10^{-15} \text{ m}^4/\text{N s}$, $c = 0.51 \pm 0.23$, $\tau_1 = 0.77 \pm 0.54 \text{ s}$, and $\tau_2 = 167 \pm 90 \text{ s}$ [77]. The results of these studies suggest that the viscoelasticity of cartilage in compression is dominated by flow-dependent effects, though the intrinsic viscoelasticity of the solid matrix is not necessarily negligible.

Static torsional tests on cylindrical disks of immature bovine cartilage (Fig. 2) have yielded a shear modulus $\mu = 0.17 \pm 0.06 \text{ MPa}$ [34]. Under oscillatory torsional testing, the shear modulus has been observed to increase with increasing loading frequency, and with axial compressive strain; for example, in immature bovine cartilage, the dynamic shear modulus increased from 0.2 MPa at 0.01 Hz to 0.4 MPa at 10 Hz, under 5 per cent compressive strain, and from 1.0 to 1.8 MPa at 16 per cent strain [41]. Using stress-relaxation experiments under simple shear (Fig. 2), the intrinsic viscoelasticity parameters of adult bovine cartilage have also been measured, yielding $\mu = 0.37 \pm 0.14 \text{ MPa}$, $c = 0.27 \pm 0.06$, $\tau_1 \sim 0.0005 \text{ s}$, and $\tau_2 = 376 \pm 116 \text{ s}$ [40].

For tensile testing, cartilage explants are cut into rectangular prismatic bars or dumbbell-shaped

specimens [35, 78]. The tensile modulus is highest in the superficial zone and decreases toward the deep zone [79]; for example, in human knee cartilage, E_{+Y1} decreases from ~ 21 to 1 MPa [35]. The tensile modulus is also greatest in the direction parallel to the split-line; for example, in human shoulder cartilage, $E_{+Y1} \sim 6.6$ MPa and $E_{+Y2} \sim 4.6$ MPa in the humeral head superficial zone [43]. The tensile modulus has been observed to increase significantly with strain [43, 78, 79]. When combined with osmotic loading, which places the tissue under a state of tensile swelling strain, unconfined compression experiments have yielded orthotropic tensile properties for Young's modulus and Poisson's ratio in the transitional range between tension and compression [29]; in immature bovine cartilage, for example, it has been found that $E_{+Y1} \sim 3.1$ MPa, $E_{+Y2} \sim 1.3$ MPa, and $E_{+Y3} \sim 1.4$ MPa under free-swelling conditions.

4 INTERSTITIAL FLUID PRESSURIZATION

From a tribological perspective, one of the remarkable characteristics of articular cartilage is the pressurization of its interstitial fluid upon loading, above and beyond the omnipresent osmotic pressure resulting from the negatively charged proteoglycans in the solid matrix. As the total stress in cartilage is the superposition of the hydrostatic interstitial fluid pressure and the solid matrix stress, according to equation (1), it follows that the interstitial fluid pressure contributes to the total load supported by the tissue. While this pressure remains elevated, cartilage may act as a 'self-pressurized hydrostatic bearing' [15, 80]. This pressurization can be formulated from theory and measured experimentally.

Let π represent the osmotic pressure contribution in the tissue; for example, from ideal Donnan law, $\pi = R\theta(c^+ + c^-)$, where c^+ and c^- are the concentrations of sodium and chloride ions in the interstitial fluid, respectively. These ion concentrations are related to the proteoglycan FCD via the electroneutrality condition, $c^+ = c^- + c^F$. The pressure above and beyond the osmotic pressure may be represented by $\tilde{p} \equiv p - \pi$; from a physical chemistry perspective, this expression is directly related to the chemical potential of the interstitial water. Substituting this relation into equation (1) yields $\boldsymbol{\sigma} = -\tilde{p}\mathbf{I} + \tilde{\boldsymbol{\sigma}}^e$, where $\tilde{\boldsymbol{\sigma}}^e \equiv -\pi\mathbf{I} + \boldsymbol{\sigma}^e$ represents the extra stresses in the tissue inclusive of all osmotic effects. As a side note, the osmotic modulus described earlier is related to π via $\Pi = -\partial\pi/\partial(\text{tr}E)$ [11, 29], and the 'effective' moduli of the solid matrix, which incorporate the osmotic modulus, may be construed as the moduli of $\tilde{\boldsymbol{\sigma}}^e$.

Consider the contact interface between two articular surfaces, where the unit normal vector to the interface is denoted by \mathbf{n} . The total normal load transmitted across the interface is given by

$$W = \int_A (\mathbf{n} \cdot \boldsymbol{\sigma}\mathbf{n} + p^*)dA \quad (14)$$

where A is the apparent contact area, $\mathbf{n} \cdot \boldsymbol{\sigma}\mathbf{n}$ is the normal traction component at the contact interface (which is negative in compression), and p^* is the ambient pressure outside the tissue. The load supported by the interstitial fluid pressure \tilde{p} is similarly given by

$$W^p = - \int_A (\tilde{p} - p^*)dA \quad (15)$$

The interstitial fluid load support is defined as the ratio of W^p/W [81, 82].

When cartilage is loaded, the interstitial fluid immediately pressurizes. Because of the pressure gradients, the fluid flows away from the loaded region so that the pressure slowly subsides. The magnitude and duration of interstitial fluid load support varies somewhat with the loading configuration. In confined compression, $W^p/W = 100$ per cent immediately upon loading, as the confining chamber does not allow an instantaneous change in the thickness of the tissue sample and the interstitial fluid needs time to exude. In unconfined compression, the instantaneous value of the fluid load support is [34]

$$\lim_{t \rightarrow 0^+} \frac{W^p}{W} = \frac{1}{1 + 2(H_{-A} - \lambda_2)/(H_{+A} - \lambda_2)} \quad (16)$$

This theoretical result holds whether or not intrinsic solid matrix viscoelasticity is taken into account [38]. The implication from this relation is that the disparity between tensile and compressive properties is critical to the magnitude of interstitial fluid load support in unconfined compression. When the tissue exhibits the same modulus in tension and compression, $H_{-A} = H_{+A}$, the peak value of fluid load support is only 33 per cent. However, when the tensile modulus is much greater than the compressive modulus, as in articular cartilage, $H_{+A} \gg H_{-A}$ and W^p/W approaches 100 per cent (given that $\lambda_2 \leq H_{-A}$ from stability considerations). In unconfined compression, the characteristic time constant for the pressure to subside is proportional to $a^2/H_{+A}k$, where a is the cylindrical sample radius. Theoretical analyses of cartilage contact problems, where the tissue is modelled as cylindrical or spherical layers bonded to a rigid impermeable substrate, show that the interstitial fluid pressurization also approaches 100 per cent in the early time response to loading

[83–86]. If the contact area is migrating on the articular layers, the fluid pressurization does not subside under steady-state rolling or sliding conditions and remains elevated at all times [87].

Cartilage interstitial fluid pressurization has been measured experimentally in the configuration of confined compression [88–91] and unconfined compression [34, 92]. In these experiments, either \tilde{p} or W^p is measured at an interface between the cartilage sample and an impermeable load-bearing surface fitted with a fluid pressure transducer. Simultaneous measurements of the total applied load W , using a load cell, allow a direct experimental evaluation of the interstitial fluid load support. Excellent agreement has been observed between these experimental measurements and theoretical predictions from mixture theory [34, 90–92], as shown for a representative confined compression case in Fig. 3. These measurements confirm that interstitial fluid pressurization significantly regulates the response of cartilage in compression.

In classical hydrodynamic lubrication theories, bearing surfaces are separated by a pressurized fluid film that supports the applied normal load and reduces the frictional force. In fluid-film lubrication, the fluid load support is 100 per cent. When the fluid film becomes depleted, bearing surfaces come into direct contact, the fluid load support reduces to zero, and the lubrication typically breaks down. In articular cartilage, however, when the porous surfaces come into direct contact, a very large fraction of the applied normal load is still supported by the pressurized interstitial fluid. (This occurs because of the porous-deformable nature of cartilage; a rigid porous bearing would not exhibit the same response.) The component of the normal load which is supported by the solid matrix of the contacting articular layers is small, resulting in a negligible frictional force [15, 81, 93]. As the interstitial fluid pressure subsides, the fraction of the normal load supported by the solid matrix and the resulting frictional force concomitantly increase.

This mechanism has been formulated within the framework of mixture theory [94]. Let φ represent the fraction of the apparent contact area over which the solid matrix of the opposing cartilage surfaces are in direct contact; φ may vary over the range $0 \leq \varphi \leq (\varphi^s)^2$, where φ^s is the solid area (or volumetric) fraction of the tissue and $1 - \varphi^s$ is the tissue porosity [94]. Over the remaining area fraction, $1 - \varphi$, the applied load is supported by the interstitial fluid; the normal load supported by the solid matrix is then given by

$$W^{\text{ss}} = W - (1 - \varphi)W^p \quad (17)$$

Assuming that the friction force is mostly contributed

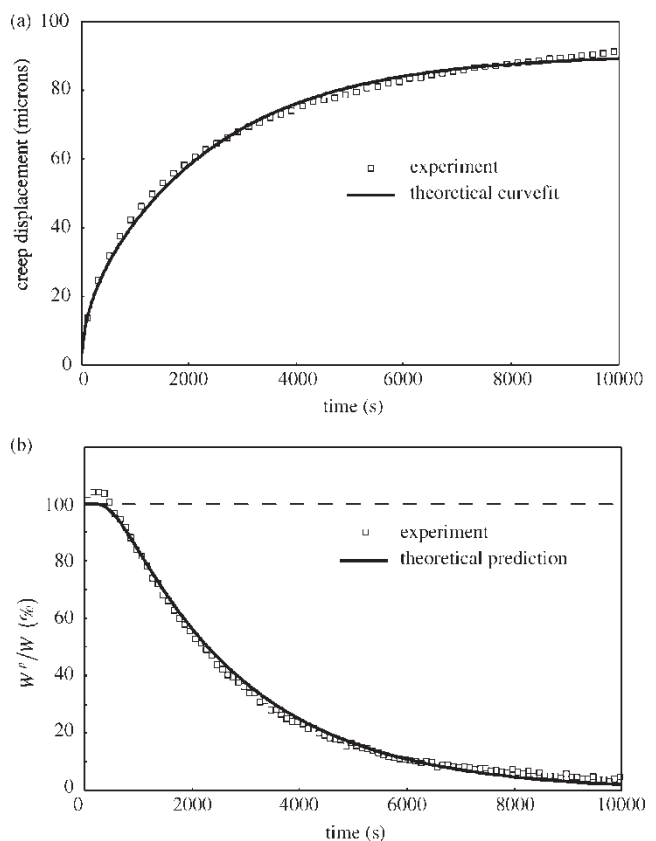


Fig. 3 (a) Axial creep displacement of bovine articular cartilage in confined compression under a constant load; the theoretical curvefit was used to determine H_A and k , and (b) Interstitial fluid load support W^p/W measured experimentally at the bottom of the test chamber; the theoretical prediction was obtained using H_A and k as determined from the creep response. Adapted with permission from Soltz and Ateshian [90]

by the contacting solid matrix, $F = \mu_{\text{eq}} W^{\text{ss}}$, the effective friction coefficient of cartilage is found to vary with interstitial fluid load support according to

$$\mu_{\text{eff}} = \frac{F}{W} = \mu_{\text{eq}} \left[1 - (1 - \varphi) \frac{W^p}{W} \right] \quad (18)$$

When the interstitial fluid load support achieves its peak value ($W^p/W \sim 1$), μ_{eff} is smallest and given by $\mu_{\text{min}} \sim \varphi \mu_{\text{eq}}$. (In the limiting case of fluid-film lubrication, $\varphi = 0$ and $\mu_{\text{min}} \sim 0$ in this idealized model, which neglects the lubricant viscosity.) Conversely, when $W^p/W = 0$, the friction coefficient achieves its equilibrium value, μ_{eq} .

This theoretical prediction has been validated experimentally in a study where the frictional response of bovine articular cartilage against glass was measured simultaneously with the interstitial fluid load support [95]. Under a step load W , the friction coefficient was

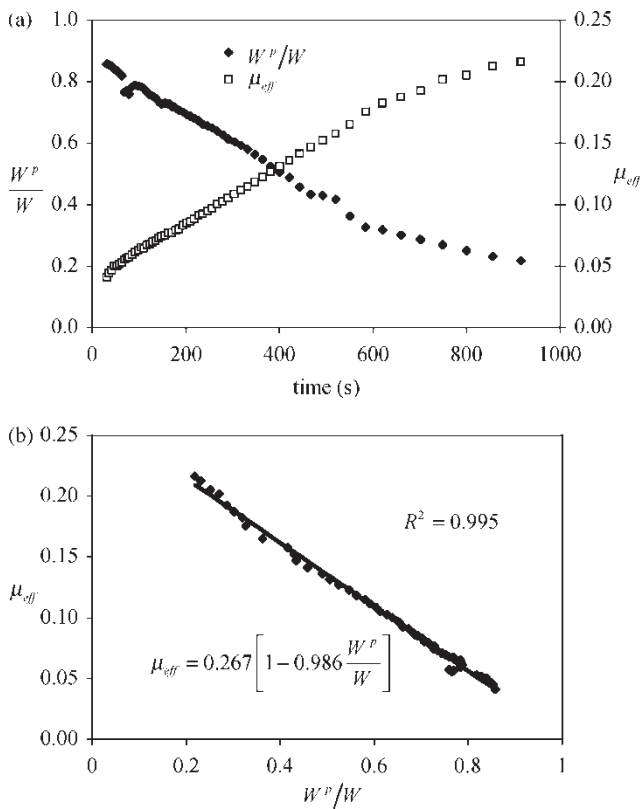


Fig. 4 (a) Simultaneous measurements of the interstitial fluid load support W^p/W and friction coefficient μ_{eff} of bovine articular cartilage against glass, under unconfined compression creep. (b) A plot of μ_{eff} versus W^p/W shows a strong linear correlation as predicted by equation (18). Data obtained from the study of Krishnan *et al.* [95]

observed to increase with time, whereas W^p/W decreased [Fig. 4(a)]. A plot of μ_{eff} versus W^p/W exhibited a linear relationship as predicted by equation (18), yielding a value of $\mu_{eq} \sim 0.28$ and $\varphi \sim 1.7$ per cent [Fig. 4(b)]. These results show very strong evidence in support of the hypothesis that the temporal response of the friction coefficient in cartilage is regulated by the interstitial fluid load support.

Measurements of interstitial fluid load support are experimentally challenging [92]; an alternative approach is to predict W^p/W from a combination of theory and experimental measurements of load and deformation. For unconfined compression of cylindrical cartilage samples under small strains, it has been shown that [96]

$$\frac{W^p}{W} = \frac{H_{+A} + \lambda_2}{H_{+A} - \lambda_2} \left[1 - \frac{W_0}{W} - \left(\frac{W_{eq} - W_0}{W} \right) \left(\frac{u - u_0}{u_{eq} - u_0} \right) \right] \quad (19)$$

The normal load W and axial deformation u may vary with time. $W_0 = W(0)$ represents the equilibrium tare load at the beginning of the test and $W_{eq} = W(t \rightarrow \infty)$ represents the equilibrium load at the end of the test, after the transient flow-dependent response has subsided; u_0 and u_{eq} similarly represent the axial deformation under tare and equilibrium conditions. This formula is valid for any loading history (such as creep or stress-relaxation), as long as equilibrium is achieved at the end of the experiment. It is based on the constitutive relation of equation (4), reduced to the case of cubic symmetry, and does not account for intrinsic viscoelasticity of the solid matrix. The term in the square brackets is determined entirely from experimental measurements. The leading coefficient depends on the material parameters H_{+A} and λ_2 ; in general, $\lambda_2 \ll H_{+A}$ in cartilage, so that this coefficient is slightly greater than unity.

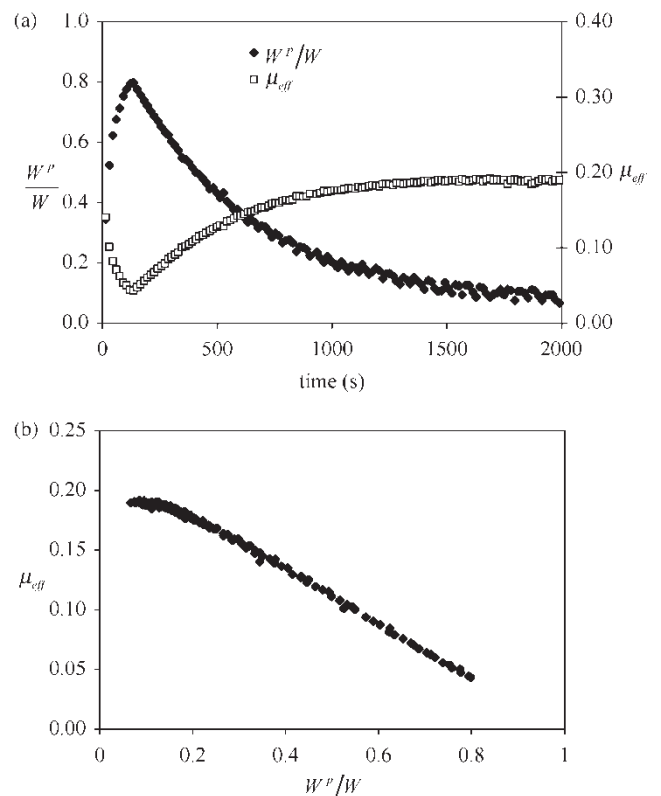


Fig. 5 (a) Interstitial fluid load support W^p/W and friction coefficient μ_{eff} of immature bovine cartilage against glass, measured in unconfined compression stress-relaxation. W^p/W is predicted from experimental measurements of load and displacement responses using equation (19). (b) A plot of μ_{eff} versus W^p/W shows a linear correlation as predicted by equation (18). Data obtained from the study of Basalo *et al.* [96]

Experimental measurements of μ_{eff} for immature bovine cartilage against glass under unconfined compression stress-relaxation [96] show that the friction coefficient decreases from μ_{eq} to a minimum value μ_{min} , whereas the axial compressive tissue strain is ramped up. When the ramp compression is stopped, the friction coefficient returns to μ_{eq} over time [Fig. 5(a)]. The interstitial fluid load support predicted from equation (19) shows a mirror trend, increasing from zero to its maximum value at the end of the ramp compression, and subsequently returning to zero [Fig. 5(a)]. Plotting μ_{eff} versus W^p/W shows a linear correlation [Fig. 5(c)], further confirming the role of interstitial fluid load support in the regulation of the cartilage friction coefficient.

5 CONCLUSION

Articular cartilage exhibits a mechanical behaviour which is significantly more complex than that of traditional bearing materials. It is a porous-hydrated tissue with very high water content, but very low hydraulic permeability. Its solid matrix exhibits tension-compression non-linearity, intrinsic viscoelasticity, and orthotropic symmetry, and its material properties are inhomogeneous through the depth of the articular layer. The diffusive drag resulting from the flow of interstitial fluid within the collagen-proteoglycan matrix produces a flow-dependent viscoelastic response. With regard to its tribological function, as the bearing material of synovial joints, the most important characteristic of articular cartilage is the pressurization of its interstitial fluid upon loading. This pressurized interstitial fluid can support most of the load transmitted across the articular layers, even though the collagen-proteoglycan matrix of the opposing surfaces come into direct contact.

Thanks to the theoretical framework of mixture theory, it has been possible to model and interpret the complex response of cartilage to loading. From this framework, it is understood that the disparity between the tensile and compressive modulus of cartilage is essential for promoting elevated interstitial fluid pressurization under various loading configurations. This finding explains the otherwise counter-intuitive observation that cartilage exhibits a much higher modulus in tension than compression, even though it is primarily subjected to compressive loads.

The framework of mixture theory has also allowed the formulation of a friction model which accounts for the unique properties of the porous-permeable articular cartilage, as summarized in equation (18). This model predicts a linear relationship between the friction coefficient of cartilage and its interstitial fluid load support, with the friction coefficient achieving its lowest value when the interstitial fluid

load support is greatest. Experimental measurements have now validated this model, demonstrating that nature has implemented an exquisite lubrication mechanism ideally suited to the loading environment of synovial joints.

Though not addressed in this review, the main degenerative disease afflicting articular cartilage is osteoarthritis, which is characterized by a loss of proteoglycans, fibrillation of the collagen matrix, increase in water content, and loss of interstitial fluid pressurization upon loading. Cartilage wear is a major characteristic of advanced osteoarthritis. The progressive changes in tribological properties of cartilage with advancing stages of disease is an active area of research.

ACKNOWLEDGEMENT

The authors would like to acknowledge the support of the National Institute of Arthritis, Musculoskeletal and Skin Diseases of the National Institutes of Health, USA (AR43628 and AR46532).

REFERENCES

- 1 Xu, L., Strauch, R. J., Ateshian, G. A., Pawluk, R. J., Mow, V. C., and Rosenwasser, M. P. Topography of the osteoarthritic thumb carpometacarpal joint and its variations with regard to gender, age, site, and osteoarthritic stage. *J. Hand Surg. Am.*, 1998, **23**(3), 454–464.
- 2 Soslowky, L. J., Flatow, E. L., Bigliani, L. U., and Mow, V. C. Articular geometry of the glenohumeral joint. *Clin. Orthop.*, 1992, **285**, 181–190.
- 3 Adam, C., Eckstein, F., Milz, S., and Putz, R. The distribution of cartilage thickness within the joints of the lower limb of elderly individuals. *J. Anat.*, 1998, **193**(Pt 2), 203–214.
- 4 Ateshian, G. A., Soslowky, L. J., and Mow, V. C. Quantitation of articular surface topography and cartilage thickness in knee joints using stereophotogrammetry. *J. Biomech.*, 1991, **24**(8), 761–776.
- 5 Rushfeldt, P. D., Mann, R. W., and Harris, W. H. Improved techniques for measuring *in vitro* the geometry and pressure distribution in the human acetabulum-I. Ultrasonic measurement of acetabular surfaces, sphericity and cartilage thickness. *J. Biomech.*, 1981, **14**(4), 253–260.
- 6 Freeman, M. A. R. *Adult articular cartilage*, 2nd edition, 1979, p. 560 (Pitman Medical, Kent).
- 7 Mow, V. C., Gu, W. Y., and Chen, F. H. Structure and function of articular cartilage and meniscus. *Basic orthopaedic biomechanics and mechano-biology* (Eds V.C. Mow and R. Huiskes) 2005, pp. 181–258 (Lippincott Williams & Wilkins, Philadelphia).
- 8 Maroudas, A. Physicochemical properties of cartilage in the light of ion exchange theory. *Biophys. J.*, 1968, **8**(5), 575–595.

- 9 **Lai, W. M., Hou, J. S., and Mow, V. C.** A triphasic theory for the swelling and deformation behaviors of articular cartilage. *J. Biomech. Eng.*, 1991, **113**(3), 245–258.
- 10 **Overbeek, J. T.** The Donnan equilibrium. *Prog. Biophys. Biophys. Chem.*, 1956, **6**, 57–84.
- 11 **Ateshian, G. A., Chahine, N. O., Basalo, I. M., and Hung, C. T.** The correspondence between equilibrium biphasic and triphasic material properties in mixture models of articular cartilage. *J. Biomech.*, 2004, **37**(3), 391–400.
- 12 **Stockwell, R. A. and Barnett, C. H.** Changes in permeability of articular cartilage with age. *Nature*, 1964, **201**, 835–836.
- 13 **Maroudas, A. and Bullough, P.** Permeability of articular cartilage. *Nature*, 1968, **219**(160), 1260–1261.
- 14 **Mansour, J. M. and Mow, V. C.** The permeability of articular cartilage under compressive strain and at high pressures. *J. Bone Jt Surg. Am.*, 1976, **58**(4), 509–516.
- 15 **McCutchen, C. W.** The frictional properties of animal joints. *Wear*, 1962, **5**, 1–17.
- 16 **Zarek, J. M. and Edward, J.** The stress-structure relationship in articular cartilage. *Med. Electron. Biol. Eng.*, 1963, **1**, 497–507.
- 17 **Mow, V. C., Kuei, S. C., Lai, W. M., and Armstrong, C. G.** Biphasic creep and stress relaxation of articular cartilage in compression: theory and experiments. *J. Biomech. Eng.*, 1980, **102**(1), 73–84.
- 18 **Truesdell, C.** The rational mechanics of materials. *Continuum mechanics II*, 1965, pp. 293–305 (Gordon & Breach, New York).
- 19 **Bowen, R. M.** In *Continuum physics* (Ed. A.E. Eringen), 1976, pp. 1–127 (Academic Press, New York).
- 20 **Bowen, R. M.** Incompressible porous media models by use of the theory of mixtures. *Int. J. Eng. Sci.*, 1980, **18**(9), 1129–1148.
- 21 **Gu, W. Y., Lai, W. M., and Mow, V. C.** A mixture theory for charged-hydrated soft tissues containing multi-electrolytes: passive transport and swelling behaviors. *J. Biomech. Eng.*, 1998, **120**(2), 169–180.
- 22 **Huyghe, J. M. and Janssen, J. D.** Quadriphasic mechanics of swelling incompressible porous media. *Int. J. Eng. Sci.*, 1997, **35**(8), 793–802.
- 23 **Lai, W. M., Mow, V. C., and Roth, V.** Effects of nonlinear strain-dependent permeability and rate of compression on the stress behavior of articular cartilage. *J. Biomech. Eng.*, 1981, **103**(2), 61–66.
- 24 **Mak, A. F., Lai, W. M., and Mow, V. C.** Biphasic indentation of articular cartilage—I. Theoretical analysis. *J. Biomech.*, 1987, **20**(7), 703–714.
- 25 **Mow, V. C., Gibbs, M. C., Lai, W. M., Zhu, W. B., and Athanasiou, K. A.** Biphasic indentation of articular cartilage—II. A numerical algorithm and an experimental study. *J. Biomech.*, 1989, **22**(8–9), 853–861.
- 26 **Athanasiou, K. A., Rosenwasser, M. P., Buckwalter, J. A., Malinin, T. I., and Mow, V. C.** Interspecies comparisons of in situ intrinsic mechanical properties of distal femoral cartilage. *J. Orthop. Res.*, 1991, **9**(3), 330–340.
- 27 **Kempson, G. E., Freeman, M. A., and Swanson, S. A.** Tensile properties of articular cartilage. *Nature*, 1968, **220**(172), 1127–1128.
- 28 **Armstrong, C. G. and Mow, V. C.** Variations in the intrinsic mechanical properties of human articular cartilage with age, degeneration, and water content. *J. Bone Jt Surg. Am.*, 1982, **64**(1), 88–94.
- 29 **Chahine, N. O., Wang, C. C., Hung, C. T., and Ateshian, G. A.** Anisotropic strain-dependent material properties of bovine articular cartilage in the transitional range from tension to compression. *J. Biomech.*, 2004, **37**(8), 1251–1261.
- 30 **Laasanen, M. S., Toyras, J., Korhonen, R. K., Rieppo, J., Saarakkala, S., Nieminen, M. T., Hirvonen, J., and Jurvelin, J. S.** Biomechanical properties of knee articular cartilage. *Biorheology*, 2003, **40**(1–3), 133–140.
- 31 **Lanir, Y.** Biorheology and fluid flux in swelling tissues, II. Analysis of unconfined compressive response of transversely isotropic cartilage disc. *Biorheology*, 1987, **24**(2), 189–205.
- 32 **Cohen, B., Lai, W. M., and Mow, V. C.** A transversely isotropic biphasic model for unconfined compression of growth plate and chondroepiphysis. *J. Biomech. Eng.*, 1998, **120**(4), 491–496.
- 33 **Soulhat, J., Buschmann, M. D., and Shirazi-Adl, A.** A fibril-network-reinforced biphasic model of cartilage in unconfined compression. *J. Biomech. Eng.*, 1999, **121**(3), 340–347.
- 34 **Soltz, M. A. and Ateshian, G. A.** A conewise linear elasticity mixture model for the analysis of tension–compression nonlinearity in articular cartilage. *J. Biomech. Eng.*, 2000, **122**(6), 576–586.
- 35 **Akizuki, S., Mow, V. C., Muller, F., Pita, J. C., Howell, D. S., and Manicourt, D. H.** Tensile properties of human knee joint cartilage: I. Influence of ionic conditions, weight bearing, and fibrillation on the tensile modulus. *J. Orthop. Res.*, 1986, **4**(4), 379–392.
- 36 **Wang, C. C., Chahine, N. O., Hung, C. T., and Ateshian, G. A.** Optical determination of anisotropic material properties of bovine articular cartilage in compression. *J. Biomech.*, 2003, **36**(3), 339–353.
- 37 **Curnier, A., He, Q. C., and Zysset, P.** Conewise linear elastic materials. *J. Elasticity*, 1995, **37**, 1–38.
- 38 **Huang, C. Y., Mow, V. C., and Ateshian, G. A.** The role of flow-independent viscoelasticity in the biphasic tensile and compressive responses of articular cartilage. *J. Biomech. Eng.*, 2001, **123**(5), 410–417.
- 39 **Hayes, W. C. and Bodine, A. J.** Flow-independent viscoelastic properties of articular cartilage matrix. *J. Biomech.*, 1978, **11**(8,9), 407–419.
- 40 **Sirt, A. A., Mak, A. F., and Wassell, R. P.** Nonlinear viscoelastic properties of articular cartilage in shear. *J. Orthop. Res.*, 1989, **7**(1), 43–49.
- 41 **Zhu, W., Mow, V. C., Koob, T. J., and Eyre, D. R.** Viscoelastic shear properties of articular cartilage and the effects of glycosidase treatments. *J. Orthop. Res.*, 1993, **11**(6), 771–781.
- 42 **Woo, S. L., Simon, B. R., Kuei, S. C., and Akeson, W. H.** Quasi-linear viscoelastic properties of normal articular cartilage. *J. Biomech. Eng.*, 1980, **102**(2), 85–90.
- 43 **Huang, C. Y., Stankiewicz, A., Ateshian, G. A., and Mow, V. C.** Anisotropy, inhomogeneity, and tension–compression nonlinearity of human glenohumeral cartilage in finite deformation. *J. Biomech.*, 2005, **38**(4), 799–809.

- 44 **Mak, A. F.** The apparent viscoelastic behavior of articular cartilage – the contributions from the intrinsic matrix viscoelasticity and interstitial fluid flows. *J. Biomech. Eng.*, 1986, **108**(2), 123–130.
- 45 **Setton, L. A., Zhu, W., and Mow, V. C.** The biphasic poroviscoelastic behavior of articular cartilage: role of the surface zone in governing the compressive behavior. *J. Biomech.*, 1993, **26**(4–5), 581–592.
- 46 **Suh, J. K. and Bai, S.** Finite element formulation of biphasic poroviscoelastic model for articular cartilage. *J. Biomech. Eng.*, 1998, **120**(2), 195–201.
- 47 **Fung, Y. C.** Biomechanics: mechanical properties of living tissues. 1981, vol. xii, p. 433 (Springer-Verlag, New York).
- 48 **Narmoneva, D. A., Wang, J. Y., and Setton, L. A.** A non-contacting method for material property determination for articular cartilage from osmotic loading. *Biophys. J.*, 2001, **81**(6), 3066–3076.
- 49 **Gu, W. Y., Yao, H., Huang, C. Y., and Cheung, H. S.** New insight into deformation-dependent hydraulic permeability of gels and cartilage, and dynamic behavior of agarose gels in confined compression. *J. Biomech.*, 2003, **36**(4), 593–598.
- 50 **Elmore, S. M., Sokoloff, L., Norris, G., and Carmeci, P.** Nature of imperfect elasticity of articular cartilage. *J. Appl. Physiol.*, 1963, **18**, 393–396.
- 51 **Sokoloff, L.** Elasticity of aging cartilage. *Fed. Proc.*, 1966, **25**(3), 1089–1095.
- 52 **Kempson, G. E., Freeman, M. A., and Swanson, S. A.** The determination of a creep modulus for articular cartilage from indentation tests of the human femoral head. *J. Biomech.*, 1971, **4**(4), 239–250.
- 53 **Hayes, W. C., Keer, L. M., Herrmann, G., and Mockros, L. F.** A mathematical analysis for indentation tests of articular cartilage. *J. Biomech.*, 1972, **5**(5), 541–551.
- 54 **Lu, X. L., Sun, D. D., Guo, X. E., Chen, F. H., Lai, W. M., and Mow, V. C.** Indentation determined mechanochemical properties and fixed charge density of articular cartilage. *Ann. Biomed. Eng.*, 2004, **32**(3), 370–379.
- 55 **Athanasίου, K. A., Niederauer, G. G., and Schenck, R. C. Jr.** Biomechanical topography of human ankle cartilage. *Ann. Biomed. Eng.*, 1995, **23**(5), 697–704.
- 56 **Athanasίου, K. A., Agarwal, A., Muffoletto, A., Dzida, F. J., Constantinides, G., and Clem, M.** Biomechanical properties of hip cartilage in experimental animal models. *Clin. Orthop.*, 1995, **316**, 254–266.
- 57 **Athanasίου, K. A., Agarwal, A., and Dzida, F. J.** Comparative study of the intrinsic mechanical properties of the human acetabular and femoral head cartilage. *J. Orthop. Res.*, 1994, **12**(3), 340–349.
- 58 **Froimson, M. I., Ratcliffe, A., Gardner, T. R., and Mow, V. C.** Differences in patellofemoral joint cartilage material properties and their significance to the etiology of cartilage surface fibrillation. *Osteoarthritis Cartilage*, 1997, **5**(6), 377–386.
- 59 **Bae, W. C., Temple, M. M., Amiel, D., Coutts, R. D., Niederauer, G. G., and Sah, R. L.** Indentation testing of human cartilage: sensitivity to articular surface degeneration. *Arthritis Rheum.*, 2003, **48**(12), 3382–3394.
- 60 **Palmer, J. L., Bertone, A. L., Malemud, C. J., and Mansour, J.** Biochemical and biomechanical alterations in equine articular cartilage following an experimentally-induced synovitis. *Osteoarthritis Cartilage*, 1996, **4**(2), 127–137.
- 61 **Grodzinsky, A. J., Lipshitz, H., and Glimcher, M. J.** Electromechanical properties of articular cartilage during compression and stress relaxation. *Nature*, 1978, **275**(5679), 448–450.
- 62 **Lee, R. C., Frank, E. H., Grodzinsky, A. J., and Roylance, D. K.** Oscillatory compressional behavior of articular cartilage and its associated electromechanical properties. *J. Biomech. Eng.*, 1981, **103**(4), 280–292.
- 63 **Brown, T. D. and Singerman, R. J.** Experimental determination of the linear biphasic constitutive coefficients of human fetal proximal femoral chondroepiphysis. *J. Biomech.*, 1986, **19**(8), 597–605.
- 64 **Armstrong, C. G., Lai, W. M., and Mow, V. C.** An analysis of the unconfined compression of articular cartilage. *J. Biomech. Eng.*, 1984, **106**(2), 165–173.
- 65 **Mizrahi, J., Maroudas, A., Lanir, Y., Ziv, I., and Webber, T. J.** The ‘instantaneous’ deformation of cartilage: effects of collagen fiber orientation and osmotic stress. *Biorheology*, 1986, **23**(4), 311–330.
- 66 **Gray, M. L., Pizzanelli, A. M., Grodzinsky, A. J., and Lee, R. C.** Mechanical and physicochemical determinants of the chondrocyte biosynthetic response. *J. Orthop. Res.*, 1988, **6**(6), 777–792.
- 67 **Sah, R. L., Kim, Y. J., Doong, J. Y., Grodzinsky, A. J., Plaas, A. H., and Sandy, J. D.** Biosynthetic response of cartilage explants to dynamic compression. *J. Orthop. Res.*, 1989, **7**(5), 619–636.
- 68 **Setton, L. A., Mow, V. C., and Howell, D. S.** Mechanical behavior of articular cartilage in shear is altered by transection of the anterior cruciate ligament. *J. Orthop. Res.*, 1995, **13**(4), 473–482.
- 69 **Gu, W. Y., Mao, X. G., Foster, R. J., Weidenbaum, M., Mow, V. C., and Rawlins, B. A.** The anisotropic hydraulic permeability of human lumbar annulus fibrosus. Influence of age, degeneration, direction, and water content. *Spine*, 1999, **24**(23), 2449–2455.
- 70 **Maroudas, A.** Physicochemical properties of articular cartilage. *Adult articular cartilage* (Ed. M. A. R. Freeman), 1979, pp. 215–290 (Pitman Medical, Kent).
- 71 **Lai, W. M. and Mow, V. C.** Drag-induced compression of articular cartilage during a permeation experiment. *Biorheology*, 1980, **17**(1,2), 111–123.
- 72 **Schinagl, R. M., Gurskis, D., Chen, A. C., and Sah, R. L.** Depth-dependent confined compression modulus of full-thickness bovine articular cartilage. *J. Orthop. Res.*, 1997, **15**(4), 499–506.
- 73 **Jurvelin, J. S., Buschmann, M. D., and Hunziker, E. B.** Optical and mechanical determination of Poisson’s ratio of adult bovine humeral articular cartilage. *J. Biomech.*, 1997, **30**(3), 235–241.
- 74 **Wong, M., Ponticello, M., Kovanen, V., and Jurvelin, J. S.** Volumetric changes of articular cartilage during stress relaxation in unconfined compression. *J. Biomech.*, 2000, **33**(9), 1049–1054.
- 75 **Wang, C. C., Deng, J. M., Ateshian, G. A., and Hung, C. T.** An automated approach for direct measurement of two-dimensional strain distributions within articular cartilage under unconfined compression. *J. Biomech. Eng.*, 2002, **124**(5), 557–567.

- 76 Korhonen, R. K., Laasanen, M. S., Toyras, J., Lappalainen, R., Helminen, H. J., and Jurvelin, J. S. Fibril reinforced poroelastic model predicts specifically mechanical behavior of normal, proteoglycan depleted and collagen degraded articular cartilage. *J. Biomech.*, 2003, **36**(9), 1373–1379.
- 77 Huang, C. Y., Soltz, M. A., Kopacz, M., Mow, V. C., and Ateshian, G. A. Experimental verification of the roles of intrinsic matrix viscoelasticity and tension–compression nonlinearity in the biphasic response of cartilage. *J. Biomech. Eng.*, 2003, **125**(1), 84–93.
- 78 Woo, S. L., Akeson, W. H., and Jemmott, G. F. Measurements of nonhomogeneous, directional mechanical properties of articular cartilage in tension. *J. Biomech.*, 1976, **9**(12), 785–791.
- 79 Kempson, G. E. Mechanical properties of articular cartilage. *J. Physiol.*, 1972, **223**(1), 23p.
- 80 McCutchen, C. W. Sponge-hydrostatic and weeping bearings. *Nature*, 1959, **184**, 1284.
- 81 Ateshian, G. A. A theoretical formulation for boundary friction in articular cartilage. *J. Biomech. Eng.*, 1997, **119**(1), 81–86.
- 82 Ateshian, G. A., Soltz, M. A., Mauck, R. L., Basalo, I. M., Hung, C. T., and Lai, W. M. The role of osmotic pressure and tension–compression nonlinearity in the frictional response of articular cartilage. *Transport Porous Med.*, 2003, **50**, 5–33.
- 83 Ateshian, G. A., Lai, W. M., Zhu, W. B., and Mow, V. C. An asymptotic solution for the contact of two biphasic cartilage layers. *J. Biomech.*, 1994, **27**(11), 1347–1360.
- 84 Kelkar, R. and Ateshian, G. A. Contact creep of biphasic cartilage layers. *J. Appl. Mech. Trans. ASME*, 1999, **66**(1), 137–145.
- 85 Macirowski, T., Tepic, S., and Mann, R. W. Cartilage stresses in the human hip joint. *J. Biomech. Eng.*, 1994, **116**(1), 10–18.
- 86 Krishnan, R., Park, S., Eckstein, F., and Ateshian, G. A. Inhomogeneous cartilage properties enhance superficial interstitial fluid support and frictional properties, but do not provide a homogeneous state of stress. *J. Biomech. Eng.*, 2003, **125**(5), 569–577.
- 87 Ateshian, G. A. and Wang, H. A theoretical solution for the frictionless rolling contact of cylindrical biphasic articular cartilage layers. *J. Biomech.*, 1995, **28**(11), 1341–1355.
- 88 Oloyede, A. and Broom, N. Stress-sharing between the fluid and solid components of articular cartilage under varying rates of compression. *Connect Tissue Res.*, 1993, **30**(2), 127–141.
- 89 Oloyede, A. and Broom, N. D. Is classical consolidation theory applicable to articular cartilage deformation? *Clin. Biomech.*, 1991, **6**, 206–212.
- 90 Soltz, M. A. and Ateshian, G. A. Experimental verification and theoretical prediction of cartilage interstitial fluid pressurization at an impermeable contact interface in confined compression. *J. Biomech.*, 1998, **31**(10), 927–934.
- 91 Soltz, M. A. and Ateshian, G. A. Interstitial fluid pressurization during confined compression cyclical loading of articular cartilage. *Ann. Biomed. Eng.*, 2000, **28**(2), 150–159.
- 92 Park, S., Krishnan, R., Nicoll, S. B., and Ateshian, G. A. Cartilage interstitial fluid load support in unconfined compression. *J. Biomech.*, 2003, **36**(12), 1785–1796.
- 93 Forster, H. and Fisher, J. The influence of loading time and lubricant on the friction of articular cartilage. *Proc. Instn Mech. Engrs, Part H: J. Engineering in Medicine*, 1996, **210**(H2), 109–119.
- 94 Ateshian, G. A., Wang, H., and Lai, W. M. The role of interstitial fluid pressurization and surface porosities on the boundary friction of articular cartilage. *J. Tribol.*, 1998, **120**, 241–251.
- 95 Krishnan, R., Kopacz, M., and Ateshian, G. A. Experimental verification of the role of interstitial fluid pressurization in cartilage lubrication. *J. Orthop. Res.*, 2004, **22**, 565–570.
- 96 Basalo, I. M., Raj, D., Krishnan, R., Chen, F. H., Hung, C. T., and Ateshian, G. A. Effects of enzymatic degradation on the frictional response of articular cartilage in stress relaxation. *J. Biomech.*, 2005, **38**(6), 1343–1349.

APPENDIX

Notation

A	apparent contact area
A_a	texture tensor
a_a	texture vector
c	relaxation function parameter
c^*	external bath concentration
c^+, c^-	counter-ion concentrations
c_r^F, c^F	fixed-charge density
D^+, D^-	counter-ion diffusivities
E	strain tensor
E_i	exponential integral function
$E_Y, E_{\pm Y}, E_{\pm Ya}$	Young's moduli
$E_{\pm Y}^{0+}$	instantaneous Young's moduli
F	friction force
f	dynamic loading frequency
f_c	characteristic frequency
g	relaxation function
$H_A, H_{\pm A}, H_{\pm Aa}$	aggregate moduli
I	identity tensor
k, k_0, k_a	hydraulic permeability
M	permeability function parameter
n	contact interface unit normal
p, \tilde{p}	interstitial fluid pressure
p^*	external bath ambient pressure
R	universal gas constant
u	solid matrix displacement
u, u_0, u_{eq}	axial solid displacement
v^s	solid matrix velocity
W, W_0, W_{eq}	normal load

W^p	load supported by fluid pressure	Π	osmotic modulus
\mathbf{w}	interstitial fluid flux	π	osmotic pressure
θ	absolute temperature	$\boldsymbol{\sigma}$	total stress tensor
$\lambda, \lambda_{\pm 1}, \lambda_2, \lambda_{\pm aa}, \lambda_{ab}$	elastic moduli	$\boldsymbol{\sigma}^e, \tilde{\boldsymbol{\sigma}}^e$	extra stress tensor
μ, μ_a	shear moduli	$\boldsymbol{\sigma}^{ve}$	viscoelastic extra stress tensor
$\mu_{eff}, \mu_{eq}, \mu_{min}$	friction coefficients	τ_1, τ_2	relaxation function parameters
ν, ν_{\pm}	Poisson's ratios	φ	contact area fraction
ν_{\pm}^{0+}	instantaneous Poisson's ratios	φ^s	solid fraction
		φ_r^w	tissue porosity